Multi-Tone Active Noise Equalizer With Spatially Distributed User-Selected Profiles

Miguel Ferrer, *Member, IEEE*, Maria de Diego, *Senior Member, IEEE*, Amin Hassani, *Senior Member, IEEE*, Marc Moonen, *Fellow, IEEE*, Gema Piñero, *Senior Member, IEEE*, and Alberto Gonzalez, *Senior Member, IEEE*

***Abstract*—In work we propose a multi-channel active noise equalizer (ANE) that can deal with multi-frequency noise signals and assigns simultaneously different equalization gains to each frequency component at each monitoring sensor. For this purpose, we state a pseudo-error noise signal for each sensor of the ANE, which has to be cancelled out in order to get the desired equalization profiles. Firstly, the optimal analytic solution for the ANE filters in the case of single-frequency noise is provided, and an adaptive algorithm based on the Least Mean Squared (LMS) is proposed for the same case. We also show that this adaptive strategy reaches the theoretical solution in steady state. Secondly, we state an equivalent approach for the case of multi-frequency noise based on two alternatives: a common pseudo-error signal at each sensor for all frequencies, and a different pseudo-error signal at each sensor for each frequency. The analytic and adaptive solutions for the ANE control filters have been developed for both pseudo-error alternatives. Finally, the ability of the proposed ANE to achieve simultaneously different user-selected noise profiles in different locations has been validated by their transfer functions and simulations.**

***Index Terms*—Active noise control, active noise equalization, multi-tone noise, spatially distributed ANE, user-selected noise profile.**

I. Introduction and Problem Statement

MANY of the acoustic noises that affect our daily lives are due to mechanical systems that generate noises with periodic components, like for instance household appliances, trains or car diesel and gas engines. These periodic components are related to the rotational speed [1] of the mechanical device and are usually very annoying. Therefore, systems that can cancel them, or at least minimize their sound level [2], [3], [4], [5], [6], [7], [8], [9] or their perceived annoyance [10], [11], [12], [13], [14], or even equalize the noise [15], [15], [16], [17], [18], [19], are required.

Many efforts have been made to improve these techniques: analyzing their convergence [20], adding mechanisms for on-line detection of noise frequencies [21], [22], getting better frequency resolution when the frequency separation between two adjacent tones is small [23], correcting the mismatch at those frequencies [24], [25], [26], or considering non-linearities [27]. Nevertheless all of them deal with single-channel systems, or multi-channel systems [28], [29], [30], where each control point is not independently considered.

Some real life situations require simultaneously different noise profiles at different locations within an enclosure, which gives rise to the need of a personalized active equalization of the multifrequency noise at each position. In this sense, Fig. 1 shows a system with K control points or sensors where a particular gain is required at each sensor position. The primary noise signal generated by the noise source, $x(n) = A_{ref}\cos(\omega_0 n + \phi_{ref})$, arrives at each kth sensor filtered through the acoustic path between this noise signal and the sensor, $p_k(n)$, which is usually modelled as a Finite Impulse Response (FIR) filter and it is called primary acoustic path. We call $d_k(n)$ the noise signal that is recorded at each sensor, $d_k(n) = x(n) * p_k(n)$, where $*$

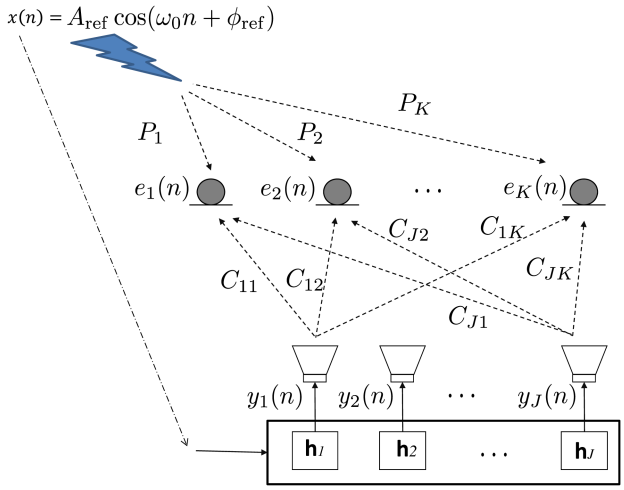

Fig. 1. Multi-channel system (K error sensors and J loudspeakers) for the active control of a single tonal noise using a single reference signal.

Manuscript received 6 July 2022; accepted 25 September 2022. Date of publication 10 October 2022; date of current version 14 October 2022. This work was supported by EU jointly with Spanish Government and Generalitat Valenciana under Grants RTI2018-098085-BC41, PID2021-125736OB-I00 (MCIU/AEI/FEDER), RE D2018-102668-T, and PROMETEO/2019/109. The associate editor coordinating the review of this manuscript and approving it for publication was Prof. Wenwu Wang. *(Corresponding author: Alberto Gonzalez.)*

Miguel Ferrer, Maria de Diego, Gema Piñero, and Alberto Gonzalez are with the Institute of Telecommunications and Multimedia Applications (iTEAM), Universitat Politècnica de València (UPV), 46022 Valencia, Spain (e-mail: mferrer@dcom.upv.es; mdediego@dcom.upv.es; gpinyero@iteam.upv.es; agonzal@dcom.upv.es).

Amin Hassani and Marc Moonen are with the STADIUS Center for Dynamical Systems, Signal Processing and Data Analytics, KU Leuven, 3000 Leuven, Belgium (e-mail: amin.hassani@esat.kuleuven.be; marc.moonen@esat.kuleuven.be).

Digital Object Identifier 10.1109/TASLP.2022.3212833

stands for the convolution operation. Without loss of generality, we assume at this point that the original noise contains only the frequency f_0 with $\omega_0 = 2\pi f_0$. However, in Section III we will extend the analysis to noise sources whose spectral content includes multiple frequencies. As said before, the system should provide a particular noise profile at each sensor. For this purpose, J secondary sources or loudspeakers are used, whose output signals $y_j(n), j = 1, \ldots, J$, result from filtering the noise signal $x(n)$ through a filter $\mathbf{h}_j$, as shown in Fig. 1. It should be noted that the reference signal of the system and the noise that is emitted by the source are assumed to be the same signal $x(n)$ in Fig. 1. In case that the reference signal differs in amplitude or phase from the original noise, the proposed model would still be valid by simply including the phase and amplitude differences within the phase and amplitude of their respective primary transfer functions, $P_k(\omega_0)$[1], $k = 1, \ldots, K$. In this sense, a reference signal can easily be synthesized just knowing the frequency of the noise signal without knowing its exact phase and amplitude.

Taking into account that the acoustic transfer function between the secondary source j and the sensor k at ω_0 is denoted by $C_{jk}(\omega_0)$, and that $P_k(\omega_0)$ is the transfer function between the original noise source and the sensor kth at the same frequency, then, using linear superposition (see Fig. 1), we can express the error signal as

$$E_k(\omega_0) = D_k(\omega_0) + \sum_{j=1}^{J} Y_j(\omega_0) C_{jk}(\omega_0), \tag{1}$$

where $Y_j(\omega_0)$ is the Fourier transform (FT) of the output signal $y_j(n)$ of loudspeaker j at ω_0. $E_k(\omega_0)$ and $D_k(\omega_0)$ are the FTs of the error signal and the desired error signal at the kth sensor respectively, both particularized for ω_0.

We also assume that a particular residual error noise signal $\widetilde{e}_k(n)$ is desired at each sensor location. Let us express this requirement on the signal picked up by the kth sensor, $e_k(n)$, such that

$$E_k(\omega_0) \rightarrow \widetilde{E}_k(\omega_0) = \beta_k D_k(\omega_0), \tag{2}$$

where $\widetilde{E}_k(\omega_0)$ is the FT of the desired error signal at the kth sensor, and β_k ($\beta_k \geq 0$ and $\beta_k \neq 1$), is a constant that sets the desired equalization profile for ω_0 at this sensor location.

Substituting (2) into (1), the following expression must be fulfilled for every sensor:

$$X(\omega_0) P_k(\omega_0)(\beta_k - 1) = \sum_{j=1}^{J} X(\omega_0) H_j(w_0) C_{jk}(\omega_0), \ \forall k, \tag{3}$$

where $X(\omega_0)$ is the FT of $x(n)$ at ω_0 that fulfills $Y_j(\omega_0) = H_j(\omega_0) X(\omega_0)$.

The equality stated in (3) can be expressed in matrix form to include all the sensors as

$$\mathbf{C}\mathbf{h} = \mathbf{p}_\beta \,, \tag{4}$$

where

$$\mathbf{C} = \begin{bmatrix} C_{11}(\omega_0) & C_{21}(\omega_0) & \cdots & C_{J1}(\omega_0) \\ C_{12}(\omega_0) & C_{22}(\omega_0) & \cdots & C_{J2}(\omega_0) \\ \vdots & \vdots & \ddots & \vdots \\ C_{1\,K}(\omega_0) & C_{2\,K}(\omega_0) & \cdots & C_{JK}(\omega_0) \end{bmatrix}, \tag{5}$$

is a matrix containing the acoustic transfer functions of the secondary paths,

$$\mathbf{h} = \begin{bmatrix} H_1(\omega_0) & H_2(\omega_0) & \cdots & H_J(\omega_0) \end{bmatrix}^T, \tag{6}$$

is a vector that contains the transfer function of the filters that feed each loudspeaker and

$$\mathbf{p}_\beta = \begin{bmatrix} (\beta_1 - 1) P_1(\omega_0) & \ldots & (\beta_K - 1) P_K(\omega_0) \end{bmatrix}^T \tag{7}$$

is a vector with the acoustic transfer functions of the primary paths weighted by the corresponding gain $(\beta_k - 1)$.

The feasibility of the scheme shown in Fig. 1 to fulfill (4) depends mostly on the acoustic system characteristics, in particular on the matrix $\mathbf{C}$. If the system has more loudspeakers than control points, $J > K$, then (4) is underdetermined and its minimum norm solution is given by

$$\mathbf{h}_{opt} = \mathbf{C}^H \left(\mathbf{C}\mathbf{C}^H \right)^{-1} \mathbf{p}_\beta \,, \tag{8}$$

as long as $\mathbf{C}$ is full rank, which becomes $\mathbf{h}_{opt} = \mathbf{C}^{-1}\mathbf{p}_\beta$, when $K = J$. If the system in (4) has more control points than loudspeakers, $K > J$, there are not enough degrees of freedom to reach the desired solution.

Considering now (4)–(7), whose solution are the filter coefficients (6) for each loudspeaker j, it is very unlikely to know or even estimate the transfer functions $P_k(\omega_0)$ in practice. However, adaptive systems do not usually know $P_k(\omega_0)$. Furthermore, adaptive strategies can evolve with changes of the initial system setup. In this work we present an adaptive strategy for the solution of (4)–(7) that provides the required attenuation β_k at each sensor position, as described in (2). We will also show that, on average, the steady-state solution of the adaptive algorithm is equal to the solution of (4). Additionally, we will extend the proposed adaptive strategy to signals composed of multiple frequencies.

The rest of the paper is organized as follows: in Section II the Minimum Mean Square pseudo Error solution for the filters $\mathbf{h}$ in (4) is obtained in closed-form, provided that the transfer functions of the primary paths $P_k(\omega_0)$ are known. Since $P_k(\omega_0)$ are usually unknown, an adaptive algorithm based on the Multiple Error Filtered-x LMS (MEFxLMS) scheme [31] is developed, together with the operating conditions to assure stability. Section III presents two strategies for the extension of the proposed algorithm to deal with multiple frequency noise profiles, while Section IV presents some relevant simulation results. Finally, Section V summarizes the conclusions. Furthermore, Appendices A and B show the development of the adaptive filtering expressions for the multi-frequency controllers, and Appendix C illustrates the steady-state analysis of both multi-frequency equalization strategies.

[1]Throughout the paper the transfer function of a system is denoted by the z-transform of the respective time impulse response particularized at $z = e^{i\omega}$.

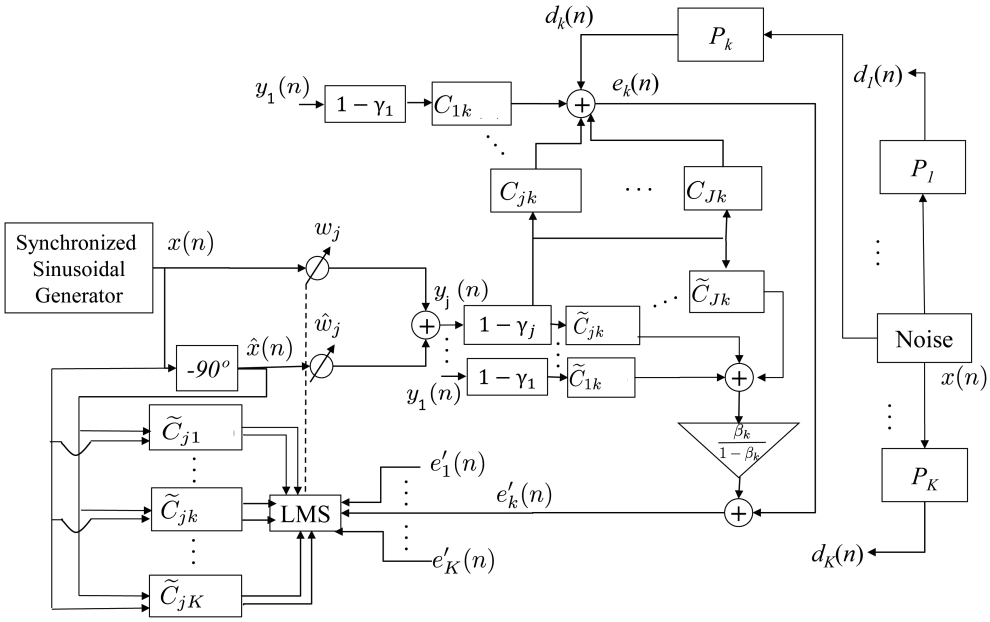

Fig. 2. Scheme of the multi-channel filtered-x LMS equalizer for the control point k and the loudspeaker j with a particular equalization factor β_k at each control point.

Throughout this paper the following notation will be used: scalars and signals are written in italic lowercase letters, a, values of the transfer functions in italic uppercase, A, vectors in lowercase and bold, $\mathbf{a}$, while matrices are shown in uppercase and bold, $\mathbf{A}$. The following symbols and operators used are: $i = \sqrt{-1}$, $\mathrm{Re}\{\cdot\}$ and $\mathrm{Im}\{\cdot\}$ are respectively the real and imaginary part of a complex number, $\mathrm{E}\{\cdot\}$ denotes the statistical mean operator and $\mathrm{tr}\{\cdot\}$ stands for the trace of a matrix. Finally, $\mathrm{diag}\{\cdot\}$ denotes a diagonal matrix whose diagonal is formed by the elements of its argument.

II. Multi-Channel ANE for Single-Frequency Noise

A multi-channel adaptive equalizer that weights a multi-frequency noise signal by an arbitrary equalization factor β_{lk} for each ω_l was presented in [30], [32]. However, the gains were assumed to be the same for all the sensors at one particular frequency, that is, $\beta_{l1} = \beta_{l2} = \cdots = \beta_{lK}$. This equalizer was based on notch adaptive filters as proposed by Kuo in [15], [16], [33]. Thus it used the adaptive strategy of filtered-x LMS [31], [34] and adapted the filter coefficients by considering each complex coefficient as two real ones, which were fed by the in-phase and quadrature components of the reference signal. Fig. 2 shows a generic scheme of this type of equalizer where the instantaneous power of the pseudo-error signal, defined as

$$e'_k(n) = e_k(n) + \frac{\beta_k}{1-\beta_k}\sum_{j=1}^{J}\{y_j(n) * \widetilde{c}_{jk}(n)\}, \qquad (9)$$

can be minimized in order to design the control filters. Here $\widetilde{c}_{jk}(n)$ represents the estimated value of the true secondary acoustic path $c_{jk}(n)$. As said before, the equalization factor β_k corresponds to ω_0 and exhibits the same value for every sensor, [30]. Although this scheme can achieve $e_k(n) = \beta_k d_k(n)$ at steady-state for the case of perfect estimation of the secondary paths, $\widetilde{c}_{jk}(n) = c_{jk}(n)$, it cannot be straightforwardly extended to the case of different equalization factors, β_k, for each sensor.

Therefore, let us assume in the following that a different equalization factor, β_k, is desired for each sensor in Fig. 2, where the "LMS" block performs the MEFxLMS algorithm. This algorithm selection is not exclusive, so different, and generally more complex, alternative adaptive strategies could be explored, as the recently proposed Recursive Least Squares based Model Predictive Control (RLSMPC) [35] or noise-robust low complexity adaptive schemes like described in [36], [37]. The system needs to know all the pseudo-error noise signals and all the signals that result from filtering the in-phase and quadrature components of the reference signal through their corresponding estimated frequency response of the secondary paths, $\widetilde{C}_{jk}$. From Fig. 2, the kth pseudo-error signal can be expressed for ω_0 as

$$E'_k(\omega_0) = E_k(\omega_0) + f(Y_1(\omega_0), C_{1\,k}(\omega_0), \ldots, Y_J(\omega_0), C_{Jk}(\omega_0)), \qquad (10)$$

where $f(\cdot)$ is a function that will be specified later, and exact knowledge of the secondary paths, $\widetilde{C}_{jk}(\omega_0) = C_{jk}(\omega_0)$, has been assumed.

Function $f(\cdot)$ in (10) should fulfil $E_k(\omega_0) \to \beta_k D_k(\omega_0)$ when $E'_k(\omega_0) = 0$. On the other hand, we can consider a more general case where the filter outputs $y_j(n)$ are weighted by a parameter $(1-\gamma_j)$ in order to control the dynamic range of the adaptive filter's output signal, which models the need in practice to deal with finite precision effects and adjust the input working range of the D/A converter. Thus the residual error signal for

each sensor can be expressed by

$$E_k(\omega_0) = D_k(\omega_0) + \sum_{j=1}^{J} (1-\gamma_j) Y_j(\omega_0) C_{jk}(\omega_0). \quad (11)$$

Note that the above expression (11) is similar to (1) except for the weight $(1-\gamma_j)$ that affects to the output signals $Y_j(\omega_0)$.

When the target has been reached, which means $E_k(\omega_0) = \beta_k D_k(\omega_0)$, the following expression is fulfilled:

$$D_k(\omega_0) = -\frac{1}{1-\beta_k} \sum_{j=1}^{J} (1-\gamma_j) Y_j(\omega_0) C_{jk}(\omega_0). \quad (12)$$

Then multiplying by β_k both sides of (12) and considering expression (10) when $E'_k(\omega_0) = 0$, the following definition for the function $f(\cdot)$ of (10) arises:

$$f(Y_1(\omega_0), C_{1\,k}(\omega_0), \ldots, Y_J(\omega_0), C_{Jk}(\omega_0)) = \frac{\beta_k}{1-\beta_k} \sum_{j=1}^{J} (1-\gamma_j) Y_j(\omega_0) C_{jk}(\omega_0), \quad (13)$$

and, consequently, the pseudo-error signal can be expressed as

$$E'_k(\omega_0) = E_k(\omega_0) + \frac{\beta_k}{1-\beta_k} \sum_{j=1}^{J} (1-\gamma_j) Y_j(\omega_0) C_{jk}(\omega_0). \quad (14)$$

The pseudo-error expression in (14) is valid for any equalization factor, except for $\beta_k = 1$, and for any $k = 1, \ldots, K$. Therefore, the algorithm exhibits no solution for those sensors whose desired equalization means to keep the noise at its original level, $E_k(\omega_0) \to D_k(\omega_0)$.

In the following subsection we will find the optimal solution for the problem of minimizing the mean power of the pseudo-error noise expressed in (14). Then, we will further state the corresponding adaptive strategy that minimizes (14) without the need of explicitly knowing the value of the noise at every sensor, $D_k(\omega_0)$, or, alternatively, their corresponding primary acoustic paths $P_k(\omega_0)$.

A. The Minimum Mean Square Pseudoerror Solution

We define the following vector formed by the components of the reference signal, $x(n) = A_{\text{ref}} \cos(\omega_0 n + \phi_{\text{ref}})$, filtered by the secondary paths $c_{jk}(n)$ as:

$$\mathbf{x}_{jk}(n) = \begin{bmatrix} A_{jk} A_{\text{ref}} \cos(\omega_0 n + \phi_{\text{ref}} + \phi_{jk}) \\ A_{jk} A_{\text{ref}} \sin(\omega_0 n + \phi_{\text{ref}} + \phi_{jk}) \end{bmatrix}, \quad (15)$$

where A_{jk} and ϕ_{jk} are the magnitude and the phase of $C_{jk}(\omega_0)$ respectively. Let us assume that the whole system is linear, thus the acoustic, c_{jk}, and electric adaptive systems can be exchanged. Then we substitute the value of $E_k(\omega_0)$ from (11) into (14) and perform the inverse FT to achieve the following expression of the pseudo-error noise signal in time domain:

$$e'_k(n) = d_k(n) + \frac{1}{1-\beta_k} \sum_{j=1}^{J} (1-\gamma_j) \mathbf{x}_{jk}^T(n) \mathbf{w}_j, \quad (16)$$

where $y_j(n)$ is generated as in Fig. 2 by filtering the reference signal through the adaptive filter given by $\mathbf{w}_j = \begin{bmatrix} w_j(\omega_0) & \hat{w}_j(\omega_0) \end{bmatrix}^T$.

The mean square of the pseudo-error signal in (16) can be expressed as $\mathrm{E}\{\mathbf{e}'(n)^T \mathbf{e}'(n)\}$, where $\mathbf{e}'(n) = \begin{bmatrix} e'_1(n) & e'_2(n) & \ldots & e'_K(n) \end{bmatrix}^T$ is composed by the samples of the K pseudo-error signals at time n. It can be shown [38] that the values of $\mathbf{w}_j$ that minimize the above mean square are given by

$$\mathbf{w}_{opt} = -\mathbf{R}^{-1} \mathbf{p}, \quad (17)$$

where $\mathbf{w}$ is defined as the $2J \times 1$ vector

$$\mathbf{w} = \begin{bmatrix} \mathbf{w}_1^T & \mathbf{w}_2^T & \ldots & \mathbf{w}_J^T \end{bmatrix}^T. \quad (18)$$

The $2J \times 2J$ correlation matrix $\mathbf{R}$ and the $2J \times 1$ cross-correlation vector $\mathbf{p}$ are respectively defined as

$$\mathbf{R} = \mathrm{E}\left\{ \sum_{k=1}^{K} \mathbf{x}_k(n) \mathbf{x}_k^T(n) \right\} = \sum_{k=1}^{K} \mathrm{E}\left\{ \mathbf{x}_k(n) \mathbf{x}_k^T(n) \right\}, \quad (19)$$

and

$$\mathbf{p} = \mathrm{E}\left\{ \sum_{k=1}^{K} \mathbf{x}_k(n) d_k(n) \right\} = \sum_{k=1}^{K} \mathrm{E}\left\{ \mathbf{x}_k(n) d_k(n) \right\}, \quad (20)$$

where the $2J \times 1$ vector $\mathbf{x}_k(n)$ is defined as

$$\mathbf{x}_k(n) = \begin{bmatrix} \frac{1-\gamma_1}{1-\beta_k} \mathbf{x}_{1\,k}^T(n) & \ldots & \frac{1-\gamma_J}{1-\beta_k} \mathbf{x}_{Jk}^T(n) \end{bmatrix}^T. \quad (21)$$

The correlation matrix $\mathbf{R}$ can be partitioned in J^2 matrices such that

$$\mathbf{R} = \begin{bmatrix} \mathbf{R}_{11} & \mathbf{R}_{12} & \ldots & \mathbf{R}_{1J} \\ \mathbf{R}_{21} & \mathbf{R}_{22} & \ldots & \mathbf{R}_{2J} \\ \vdots & & \ddots & \vdots \\ \mathbf{R}_{J1} & \mathbf{R}_{J2} & \ldots & \mathbf{R}_{JJ} \end{bmatrix}, \quad (22)$$

where the expression of each 2×2 matrix $\mathbf{R}_{fc}$ located at the fth row and cth column of the partition (22) is given by

$$\mathbf{R}_{fc} = \sum_{k=1}^{K} \frac{(1-\gamma_f)(1-\gamma_c)}{(1-\beta_k)^2} \mathrm{E}\left\{ \mathbf{x}_{fk}(n) \mathbf{x}_{ck}^T(n) \right\}. \quad (23)$$

Taking into account the expression of $\mathbf{x}_{jk}(n)$ in (15), the above matrix $\mathbf{R}_{fc}$ can be explicitly expressed as

$$\mathbf{R}_{fc} = \sum_{k=1}^{K} \frac{(1-\gamma_f)(1-\gamma_c) A_{\text{ref}}^2 A_{fk} A_{ck}}{2(1-\beta_k)^2} \cdot \times \begin{bmatrix} \cos(\phi_{fk} - \phi_{ck}) & -\sin(\phi_{fk} - \phi_{ck}) \\ \sin(\phi_{fk} - \phi_{ck}) & \cos(\phi_{fk} - \phi_{ck}) \end{bmatrix}, \quad (24)$$

where we have considered that the amplitudes A_{ref}, A_{fk}, A_{ck}, and phases ϕ_{fk}, ϕ_{ck} are known.

In a similar way, the cross-correlation vector $\mathbf{p}$ can be partitioned in J vectors such that

$$\mathbf{p} = \begin{bmatrix} \mathbf{p}_1^T & \mathbf{p}_2^T & \ldots & \mathbf{p}_J^T \end{bmatrix}^T,$$

where each 2×1 vector $\mathbf{p}_j$ is expressed as

$$\mathbf{p}_j = \sum_{k=1}^{K} \mathrm{E}\{\mathbf{x}_{jk}(n) d_k(n)\} = \sum_{k=1}^{K} \frac{A_{\text{ref}}^2 A_{jk} A_k (1-\gamma_j)}{2(1-\beta_k)} \begin{bmatrix} \cos(\phi_{jk} - \phi_k) \\ \sin(\phi_{jk} - \phi_k) \end{bmatrix}, \quad (25)$$

and where A_k and ϕ_k are the magnitude and the phase of the acoustic transfer function of the primary path $P_k(\omega_0)$ respectively. Therefore the noise signal $d_k(n)$ could be written as

$$d_k(n) = x(n) * p_k(n) = A_k A_{\text{ref}} \cos(\omega_0 n + \phi_{\text{ref}} + \phi_k). \quad (26)$$

It can be shown that the solution given by (17) is equivalent to (8) when $J = K$ and $A_{\text{ref}} = 1$. That is,

$$\mathbf{w}_{opt} = \mathbf{C}_{\boldsymbol{\gamma}}^{-1} \mathbf{p}_{\beta}, \quad (27)$$

where we define a new matrix $\mathbf{C}_{\boldsymbol{\gamma}}$ based on matrix $\mathbf{C}$ from (5) such that $\mathbf{C}_{\boldsymbol{\gamma}} = \mathbf{C}\mathrm{diag}\{\bar{\boldsymbol{\gamma}}\}$, with $\bar{\boldsymbol{\gamma}} = \begin{bmatrix} (1-\gamma_1) & (1-\gamma_2) & \cdots & (1-\gamma_J) \end{bmatrix}^T$.

Notice that the expressions for $\mathbf{R}$ expressed as (22)–(24) and $\mathbf{p}$ defined as (25) are equivalent to the previously proposed ones of Section I.

B. Adaptive Solution Based on the Least Mean Squared (LMS) Algorithm

From the expression of each cross-correlation vector $\mathbf{p}_j$ in (25), the closed-form solution to (17) can only be found if the acoustic system is completely characterized, which means knowing its primary paths, $P_k(\omega_0)$, and its secondary ones, $C_{jk}(\omega_0)$. Regarding the secondary paths, their estimate can be usually obtained through channel measurements [39], [40] (or even applying on-line estimation methods [41]). However, primary paths $P_k(\omega_0)$ can rarely be measured or known. Therefore, we propose in the following an stochastic gradient algorithm that does not need to know $P_k(\omega_0)$ to look for the optimum control filters. In particular we will use the widely known LMS algorithm [38], whose updating equation at time n for the particular system of Fig. 2 can be expressed as

$$\mathbf{w}(n) = \mathbf{w}(n-1) - \mu \nabla_{\mathbf{w}} \{(\mathbf{e}'(n))^T \mathbf{e}'(n)\}, \quad (28)$$

where $\mathbf{w}(n)$ is the same vector defined in (18) but now with an explicit dependence on the sample time n, μ is the step size to assure stability [38], $\mathbf{e}'(n)$ was defined in (II-A), and the $2J \times 1$ vector $\nabla_{\mathbf{w}}$ represents the gradient operator[2].

Taking into account the generic expression of the pseudo-error signals given by (16), the updating equation for the jth filter, $j = 1, \ldots, J$, is

$$\mathbf{w}_j(n) = \mathbf{w}_j(n-1) - 2\mu \sum_{k=1}^{K} \frac{1-\gamma_j}{1-\beta_k} \widetilde{\mathbf{x}}_{jk}(n) e'_k(n), \quad (29)$$

[2]The gradient operator is defined as: $\nabla_{\mathbf{w}} = [\frac{\partial}{\partial w_1}, \frac{\partial}{\partial \hat{w}_1}, \frac{\partial}{\partial w_2}, \frac{\partial}{\partial \hat{w}_2}, \ldots, \frac{\partial}{\partial w_J}, \frac{\partial}{\partial \hat{w}_J}]^T$.

where $\widetilde{\mathbf{x}}_{jk}$ is defined as in (15) but the true secondary paths c_{jk} have been substituted by the estimated secondary paths $\widetilde{c}_{jk}$.

In this sense, it is assumed that these estimates can be obtained with enough accuracy. It is shown in Appendix C that the filter coefficients given by (29) tend, in steady-state, to the optimum coefficients provided by (17) under the assumption of perfect estimation of these secondary paths.

C. Stability Condition of the Multi-Channel ANE LMS Algorithm

It is well known that the stability of iterative gradient algorithms depends on the step size μ. It can be shown that μ must be less than the inverse of the largest eigenvalue of the correlation matrix $\mathbf{R}$ given by (22). In the particular case of a system with one loudspeaker and one sensor, $\mathbf{R} = \mathbf{R}_{11}$, we can express the bound for μ as

$$\mu < \frac{2(1-\beta_1)^2}{A_{\text{ref}}^2 A_{11}^2 (1-\gamma_1)^2} = \mu_1. \quad (30)$$

Note that the convergence speed will reduce as $\beta \to 1$. The convergence behaviour can be explored by means of zero-pole analysis as in [32].

A lower bound for the step size that does not require the eigenvalue decomposition of matrix $\mathbf{R}$ is given for the general multi-channel case by

$$\mu < \frac{1}{\mathrm{tr}\{\mathbf{R}\}} < \mu_1, \quad (31)$$

where $\mathrm{tr}\{\mathbf{R}\}$ is the trace of $\mathbf{R}$, which can be easily computed as the sum of the elements of its main diagonal as

$$\mathrm{tr}\{\mathbf{R}\} = \sum_{j=1}^{J} \sum_{k=1}^{K} \frac{(1-\gamma_j)^2 A_{\text{ref}}^2 A_{jk}^2}{(1-\beta_k)^2}. \quad (32)$$

III. Multi-Channel ANE for Multi-Frequency Noise

In this section we will extend the adaptive solutions proposed for the multi-channel single-frequency ANE of Section II to the case of noises whose spectral content is formed by multiple frequencies. These noises are called periodic when their multiple tones are harmonic among them, but, in general, they are called multi-tone or multi-frequency noises.

In the case of a multi-channel multi-frequency ANE, the equalization factor or gain, β_{lk}, will be defined for each frequency, l, and each sensor, k; and a weighting parameter, γ_{lj}, will be defined for the output signals of each frequency, l, and each loudspeaker, j. Thus, we will define LK equalization gains and LJ control filters in an equalizer system with K sensors and J loudspeakers where L frequency components have to be controlled. According to the theoretical model, the system is composed by the linear superposition of L single-frequency systems, equivalent to the one presented in Section II, working in parallel. Thus the optimal control filter for each system is given by (27), where ω_0 is replaced by ω_l. In order to obtain the optimal control filters for multi-frequency noises, we will follow [32], where an adaptive algorithm was proposed to design a

multi-channel multi-frequency ANE with the same equalization profile for all sensors.

At this point, we will extend the notation used in Section II to deal with multi-frequency signals:

- In-phase and quadrature components of the reference noise signal are now given by

$$x(n) = \sum_{l=1}^{L} A_{\text{ref},l} \cos(\omega_l n + \phi_{\text{ref},l}), \tag{33}$$

$$\hat{x}(n) = \sum_{l=1}^{L} A_{\text{ref},l} \sin(\omega_l n + \phi_{\text{ref},l}). \tag{34}$$

- β_{lk} is the equalization gain for the kth sensor at ω_l.
- $\mathbf{w}_{lj}(n)$ is the vector formed by the two coefficients of the adaptive filter that controls the jth loudspeaker output signal at ω_l. Note that we have kept the dependence with sample time n in case the proposed solution is adaptive in time:

$$\mathbf{w}_{lj}(n) = \begin{bmatrix} w_j(\omega_l, n) & \widehat{w}_j(\omega_l, n) \end{bmatrix}^T . \tag{35}$$

- γ_{lj} is the weighting factor at the output of the jth adaptive filter for the lth frequency component.
- A_{lk} and ϕ_{lk} are respectively the magnitude and phase of the transfer function of the primary path, $P_k(\omega_l)$.
- A_{ljk} and ϕ_{ljk} are respectively the magnitude and phase of the transfer function of the secondary path $C_{jk}(\omega_l)$.
- $\widetilde{\mathbf{x}}_{ljk}(n)$ is the 2×1 vector formed by the in-phase and quadrature signals of the lth frequency component of the reference signal filtered by the estimate of the secondary path, $\widetilde{c}_{ljk}$, between loudspeaker j and sensor k at ω_l. In case that the true secondary paths c_{ljk} are available, then $\widetilde{\mathbf{x}}_{ljk}(n) = \mathbf{x}_{ljk}(n)$.

Once the new multi-frequency notation has been stated, two different strategies based on [32] are developed in the following.

A. Multi-Channel Multi-Frequency ANE Based on Common Pseudo-Error Signal

In this case we will define a pseudo-error signal per sensor but common to all the frequency components. Since the different frequency components of the signals involved are considered uncorrelated, we can follow the mathematical development described in Section II. If we apply superposition to include all the frequencies, $l = 1, \ldots, L$, the pseudo-error signal for sensor k can be expressed as

$$e'_k(n) = e_k(n) + \sum_{l=1}^{L} \sum_{j=1}^{J} \frac{1-\gamma_{lj}}{1-\beta_{lk}} \beta_{lk} \widetilde{\mathbf{x}}_{ljk}^T(n) \mathbf{w}_{lj}(n). \tag{36}$$

As detailed in Appendix A, the updating equation for the adaptive filter that feeds loudspeaker j at lth frequency can be expressed as

$$\mathbf{w}_{lj}(n) = \mathbf{w}_{lj}(n-1) - 2\mu_l \sum_{k=1}^{K} \frac{1-\gamma_{lj}}{1-\beta_{lk}} \mathbf{x}_{ljk}(n) e'_k(n) . \tag{37}$$

A bound of the step size $\mu_l, l = 1, \ldots, L$, that assures stability of the above algorithm can be calculated as in (31):

$$\mu_l \leq \frac{1}{\text{tr}\{\mathbf{R}(\omega_l)\}} , \tag{38}$$

where $\text{tr}\{\mathbf{R}(\omega_l)\}$ is now given by

$$\text{tr}\{\mathbf{R}(\omega_l)\} = \sum_{j=1}^{J} \sum_{k=1}^{K} \frac{(1-\gamma_{lj})^2 A_{\text{ref},l}^2 A_{ljk}^2}{(1-\beta_{lk})^2} . \tag{39}$$

B. Multi-Channel Multi-Frequency ANE Based on Multiple Pseudo-Error Signals

This strategy of multiple pseudo-error signals is very similar to the previous one, where a common pseudo-error signal was used. The benefit of proposing multiple pseudo-error signals, which means a different pseudo-error signal for each frequency, is the possibility of running L adaptive algorithms in parallel. Consequently, the $2J$ filter coefficients for every frequency can be computed independently for $l = 1, \ldots, L$. The update equation of the filter coefficients, derived in appendix B, is given by

$$\mathbf{w}_{lj}(n) = \mathbf{w}_{lj}(n-1) - 2\mu_l \sum_{k=1}^{K} \frac{1-\gamma_{lj}}{1-\beta_{lk}} \mathbf{x}_{ljk}(n) e'_{lk}(n) , \tag{40}$$

where μ_l for $l = 1, \ldots, L$, is given by (38)-(39) and the pseudo-error signal for sensor k and frequency l is now defined as

$$e'_{lk}(n) = e_k(n) + \frac{\beta_{lk}}{1-\beta_{lk}} \sum_{j=1}^{J} (1-\gamma_{lj}) \mathbf{x}_{ljk}^T(n) \mathbf{w}_{lj}(n). \tag{41}$$

We assume that both the noise signal and the error signal, $e_k(n)$, depend only on the single frequency component ω_l. We show in Appendix C how this assumption does not prevent the adaptive algorithm to reach, on average, the same steady state solution than that of Section III-A.

It can be seen from (40) that the adaptive algorithm based on multiple pseudo-error signals can be run as L algorithms in parallel. Each one would independently achieve the optimal solution of the single frequency system as described in Section II-A. However each of them also contributes to reach an optimal global solution for all coefficients, even for those that control other frequency components, since the pseudo-error signal in (41) has content in all frequencies. Taking into account that $\mathbf{x}_{ljk}(n)$ and $\mathbf{x}_{mjk}(n)$ are uncorrelated, the solution reached by (40) tends on average to the solution reached by (37), as shown in Appendix C.

C. Transfer Function Analysis

It is known that ANE systems can be considered linear systems under usual conditions [2]. Thus, their behavior can be characterized by the knowledge of their transfer functions over the whole working frequency range. These transfer functions, $H_k(z)$, relate the corresponding error and desired signals at each sensor as

$$E_k(z) = H_k(z) D_k(z), \quad 1 \leq k \leq K, \tag{42}$$

and they should fulfill that $H_k(e^{i\omega_l}) = \beta_{lk}$ for $D_k(e^{i\omega}) \neq 0$, $\forall l, k$. These transfer functions allow to validate the equalizer performance according to the designed specifications at the control frequencies, although they can also provide information about the behavior of the equalizer outside the frequencies of interest.

It should be noted that there exists a different transfer function for each error sensor. Unfortunately, these transfer functions only present a closed expression for single-channel systems due to the cross dependence between the transfer functions corresponding to different error sensors in a general multi-channel system, as it is shown in [32]. However, they can be numerically computed and then used to predict the behaviour of the adaptive system, both at the steady state by estimating their corresponding frequency responses, and at transient state by computing their pole moduli [42]. The transfer functions can be described by a quotient of polynomials, $N_k(z)$ and $M_k(z)$, where the denominator can be factored using the transfer function poles as

$$H_k(z) = \frac{N_k(z)}{M_k(z)} = \frac{N_k(z)}{(1-p_{k1}z^{-1})(1-p_{k2}z^{-1})\cdots(1-p_{k(2L)}z^{-1})}, \tag{43}$$

where we have considered the usual assumptions that these functions have $2L$ poles ($p_{k1}, p_{k2}, \ldots, p_{k2L}$), being L the number of control frequencies, and the denominator order is equal to the numerator order [32].

The error signal at each sensor can be estimated for a given desired (input) signal using its corresponding transfer function and a deterministic approach. Let the input noise be a complex sinusoidal signal starting at $n = 0$, denoted by: $d_k(n) = e^{i\omega_0 n}\mathrm{u}(n)$, where $\mathrm{u}(n)$ is the unit step function, then the k-th error signal is given by

$$E_k(z) = \frac{N_k(z)}{(1-e^{i\omega_0}z^{-1})(1-p_{k1}z^{-1})(1-p_{k2}z^{-1})\cdots(1-p_{k(2L)}z^{-1})}, \tag{44}$$

which can be alternatively expressed by its partial fraction expansion as

$$E_k(z) = \frac{C}{1-e^{iw_0}z^{-1}} + \frac{A_{k1}}{1-p_{k1}z^{-1}} + \cdots + \frac{A_{k(2L)}}{1-p_{k(2L)}z^{-1}}, \tag{45}$$

with $C = H_k(z)|_{z=e^{i\omega_0}} = H_k(e^{i\omega_0})$, and

$$A_{kl} = (1-p_{kl}z^{-1})\left.\frac{H_k(z)}{1-e^{i\omega_0}z^{-1}}\right|_{z=p_{kl}}. \tag{46}$$

Finally, the error signal at the k-th error sensor can be estimated as

$$e_k(n) = H_k(e^{i\omega_0})e^{i\omega_0 n}\mathrm{u}(n) + A_{k1}p_{k1}^n\mathrm{u}(n) + \cdots + A_{k(2L)}p_{k(2L)}^n\mathrm{u}(n). \tag{47}$$

Since the system can be considered causal and stable for the convergence parameter fulfilling (38), all the poles remain within the unit circle and then $e_k(n) \to H_k(e^{i\omega_0})e^{i\omega_0 n} = \beta_{lk}e^{i\omega_l n}$, when $n \to \infty$ and $\omega_0 = \omega_l$. The duration of the transient stage depends on the values of the amplitudes given by (46) and the poles of (43), which can be calculated from the transfer functions.

The poles of (43) depend on the adaptive system parameters through the transfer function. The pole moduli can be calculated from the maximum values of the transfer function absolute value. These poles, which appear as conjugated pairs, are associated with the control frequencies. Consequently the poles' phases are very close to the corresponding control frequencies' angles, which eases their search through numerical methods [42].

The transient stage duration tends to be dominated by the pole with largest modulus as shown in (47), which will be the closest one to the unit circle. Let $\rho_k^{\max}$ be the largest modulus of the poles of $H_k(z)$. We can define the effective time constant for the error signal at sensor k (47), n_ϵ, as the value of n when $\rho_k^{\max}$ has decreased to $\epsilon, then (\rho_k^{\max})^{n_\epsilon} = \epsilon \Rightarrow n_\epsilon = \frac{\ln(\epsilon)}{\ln(\rho_k^{\max})}$ (i.e. for a signal decreasing of 90%, $\epsilon \approx 0.1$). This effective time constant can be used to estimate the system transient stage duration at each error sensor.

The summation given by (47) is leaded by only two terms when the poles' moduli are very similar (and close to the unit circle) and the control frequency angles are separated enough. This fact is due to the value of $\frac{1}{1-e^{i\omega_0}z^{-1}}|_{z=p_{kl}}$ in (46), which will be large when $\omega_0 = \omega_l$ for a given l and notably smaller for the rest of control frequencies in this case. This fact allows the estimation of the transient duration of each control frequency at each error sensor by using the modulus of its corresponding pole within the k-th transfer response.

On the other hand, there exist K transfer functions (K sensors) and L control frequencies in the general case. Thus there will be $(K \times 2L)$ different poles, whose moduli can be denoted by ρ_{kl}. Each frequency component commands the convergence of two coefficients of each secondary source, therefore it can be assumed that the convergence behaviour of each pair of coefficients are mostly conditioned by the maximum pole modulus for this control frequency, which can be defined as $\rho_l = \mathrm{argmax}\{\rho_{kl}\}, \forall k$. Then the convergence behaviour of each adaptive coefficient pair can be modeled by

$$\begin{aligned} w_{jl}(n) &= w_{jl}(0) + (w_{jl}(0) - w_{jl})(\rho_l^n - 1), \\ \widehat{w}_{jl}(n) &= \widehat{w}_{jl}(0) + (\widehat{w}_{jl}(0) - \widehat{w}_{jl})(\rho_l^n - 1), \end{aligned} \tag{48}$$

where w_{jl} and $\widehat{w}_{jl}$ are the coefficient values given by (17) for the j-th secondary source.

IV. Simulation Results

The performance of the proposed adaptive strategies is illustrated in the following by numerical simulations using real data. The actual acoustic paths used in the experiments are available online at [43], but decimated to a sampling frequency of 2 kHz. The multi-channel ANE system is composed by two loudspeakers ($J = 2$, number 20 and 22 in the set-up of [43]) and two sensors ($K = 2$, number 11 and 13 in the set-up of [43]),

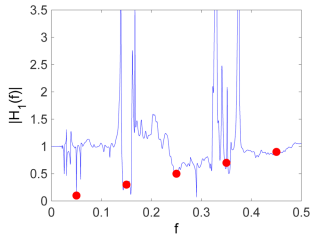

(a) Sensor #1: common pseudo-error signal.

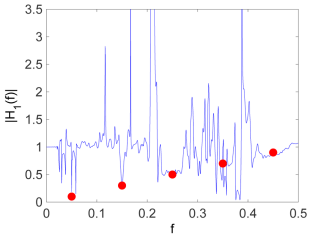

(b) Sensor #2: common pseudo-error signal.

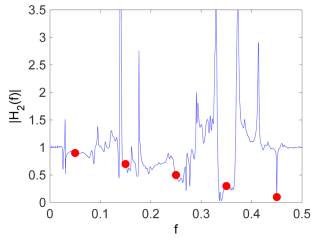

(c) Sensor #1: multiple pseudo-error signals.

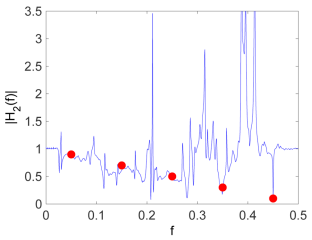

(d) Sensor #2: multiple pseudo-error signals.

Fig. 3. Magnitude of the ANE transfer functions for a system with 2 error sensors and 2 loudspeakers and different equalization profiles at each sensor. Red dots indicate the desired equalizer gains $\boldsymbol{\beta}_1$ for Sensor #1 and $\boldsymbol{\beta}_2$ for Sensor #2 at the controlled digital frequencies, $f \in \{0.05, 0.15, 0.25, 0.35, 0.45\}$.

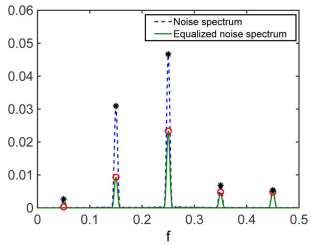

(a) Sensor #1: common pseudo-error signal.

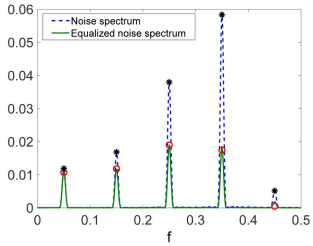

(b) Sensor #2: common pseudo-error signal.

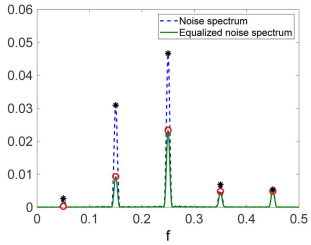

(c) Sensor #1: multiple pseudo-error signals.

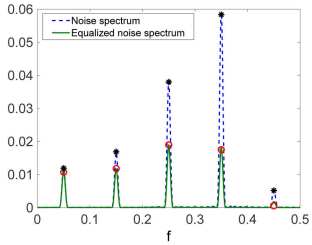

(d) Sensor #2: multiple pseudo-error signals.

Fig. 4. Spectrum of the original noise signal versus the spectrum of the error signal after convergence for each sensor and for both common and multiple error equalization profiles. Black stars indicate theoretical values of the original noise magnitudes, $|D_k(\omega_l)|$, whereas the red circles indicate those of the error signal (residual noise), $|E_k(\omega_l)|$. The controlled digital frequencies are $f \in \{0.05, 0.15, 0.25, 0.35, 0.45\}$.

and the noise to be equalized has content at five frequencies, $\{100, 300, 500, 700, 900\}$ Hz, thus $L = 5$. The convergence parameter used in all simulations was derived according to (38).

Fig. 3 shows the magnitudes of the frequency responses, $H_k(e^{i\omega})$, defined in (42), for both equalization strategies presented in Sections III-A and III-B. The sets of equalization gains, $\boldsymbol{\beta}_1 = [0.1\ 0.3\ 0.5\ 0.7\ 0.9]$ and $\boldsymbol{\beta}_2 = [0.9\ 0.7\ 0.5\ 0.3\ 0.1]$, are shown as red points at the controlled digital frequencies. It should be noted that the common pseudo-error strategy adjusts the transfer functions perfectly at the equalized frequencies, whereas the multiple pseudo-error strategy exhibits slight deviations due to the mutual influence of the filters working at different frequencies, especially those in the middle of the band, i.e., with two adjacent control frequencies.

Fig. 4 shows the spectrum of the original noise signal, $d_k(n)$, versus the spectrum of the error signal, $e_k(n)$, after algorithm convergence. The equalizer gains are the same as those used for Figure 3. The black stars indicate the theoretical values of the original noise magnitudes, $|D_k(\omega_l)|$, whereas the red circles indicate those of the theoretical error signal according to (42), $|E_k(\omega_l)| = |\beta_{lk} D_k(\omega_l)|$. All the components of the noise reference signal have an amplitude of $A_{\text{ref},l} = 1$, $\forall l$, although the magnitudes $|D_k(\omega_l)|$ are different at each sensor and frequency due to the influence of their respective primary acoustic paths. It can be observed in Figure 4 that the performance of both common and multiple pseudo-error strategies is very similar, both achieving the desired equalization profile $\beta_{lk} D_k(\omega_l)$ at each sensor.

A Gaussian white noise was added to the multi-frequency noise signal in order to test the robustness of both algorithms against the presence of broadband noise of non-tonal nature. The

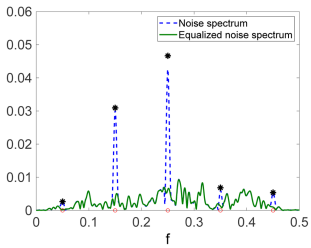

(a) Sensor #1: common pseudo-error signal.

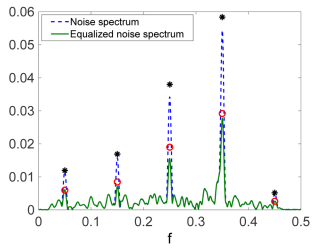

(b) Sensor #2: common pseudo-error signal.

Fig. 5. Spectrum of the original noise signal versus the spectrum of the error signal after convergence for each sensor for the common pseudo-error strategy and additive broadband noise. Black stars indicate theoretical values of the original noise magnitudes, $|D_k(\omega_l)|$, whereas the red circles indicate those of the error signal (residual noise), $|E_k(\omega_l)|$. The controlled digital frequencies are $f \in \{0.05, 0.15, 0.25, 0.35, 0.45\}$.

power ratio between the multi-frequency noise signal and the Gaussian noise was 15 dB. In this case, the equalization profile for Sensor #1 is set to $\beta_{l1} = 0, \forall l$, meaning that the system acts as an active noise canceller for that sensor, whereas $\beta_{l2} = 0.5, \forall l$, for Sensor #2. Fig. 5 shows the spectrum of the original noise signal $d_k(n)$ versus the spectrum of the error signal $e_k(n)$ for the common pseudo-error strategy, whereas Fig. 6 illustrates the temporal evolution of the adaptive filters where each filter is composed by 2 coefficients. Since both strategies behave similarly, only the results of the common error strategy have been shown in Figs. 5 and 6. It can be observed in Fig. 5 that the algorithm equalizes quite well the frequency components to

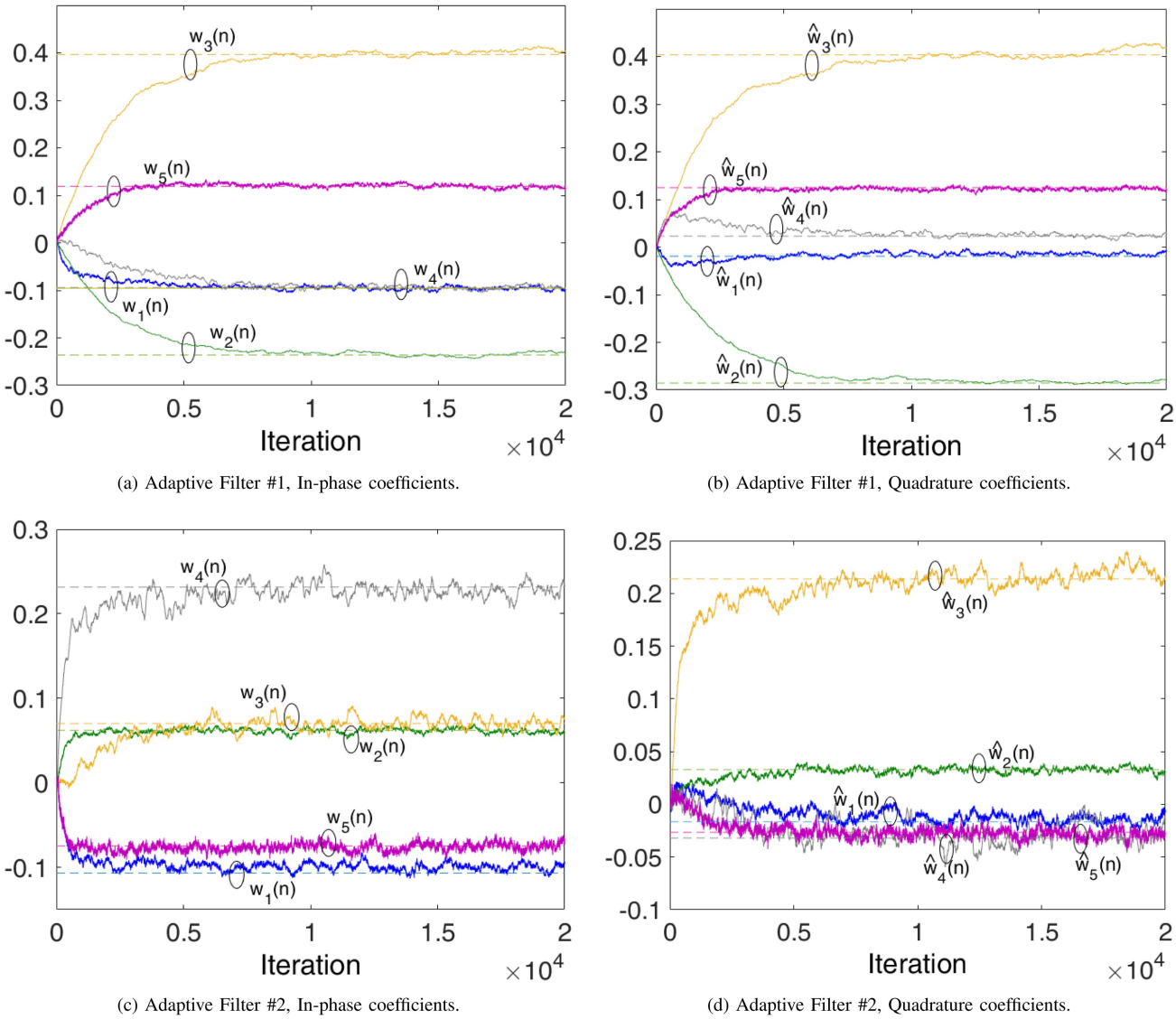

(a) Adaptive Filter #1, In-phase coefficients.

(b) Adaptive Filter #1, Quadrature coefficients.

(c) Adaptive Filter #2, In-phase coefficients.

(d) Adaptive Filter #2, Quadrature coefficients.

Fig. 6. Temporal evolution of the coefficients of both adaptive filters for the common pseudo-error strategy and additive broadband noise.

be controlled, while keeping the rest of the spectral components unaltered.

As it can be seen from Fig. 6, the coefficients move around their theoretical values with a variance proportional to the power of the added broadband noise and their corresponding convergence step. As expected, none of the proposed strategies was able to provide the desired equalization profiles at the controlled frequencies when the additive broadband noise exhibited a power higher than the multi-frequency noise signal.

Finally, we can shed some light to the transient behaviour of the proposed algorithms using the transfer functions. It has been shown that it depends on the moduli of the poles of these transfer functions. Because these multi-channel transfer functions do not have analytical expressions, they have been numerically estimated.

For $\epsilon = 0.1$, the effective time constant, n_e, for the system whose transfer functions are shown in Fig. 3 is 2302 samples for both common and multiple pseudoerror (the highest modulus of the poles found numerically was $\rho_k^{\max} = 0.999$ with a search resolution of 0.001 [42]). Fig. 7 illustrates the wave-forms of the noise signal before and after equalization. It is remarked within a square the theoretical transient stage using n_e. It can be noted that the effective time constant properly bounds the transient duration of the algorithm. Furthermore, the transient duration of each tonal noise component could be estimated by means of the maximum modulus of the poles corresponding to this component frequency due to the fact that the poles had similar modulus and the five control frequencies' angles are equispaced. As example, Fig. 8 shows the transient behaviour of the fastest and the slowest noise components (for sensor 2 and the multiple pseudoerror strategy) and their estimated transient durations, using only the magnitude of the corresponding poles for these components, which was estimated as explained in [42].

The temporal evolution of the filter coefficients could be approximated using this pole information by (48). Fig. 9 shows an example of this theoretical model compared with the simulation result for the filter coefficients that correspond to the third harmonic of the noise signal. It can be seen that this simple

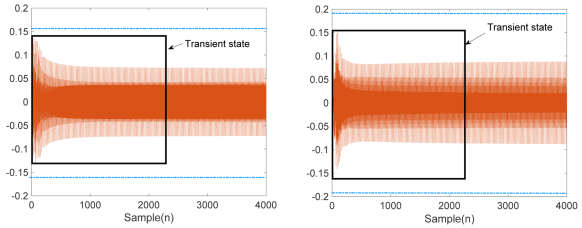

(a) Sensor #1: common pseudo-error signal.

(b) Sensor #2: common pseudo-error signal.

(c) Sensor #1: multiple pseudo-error signals.

(d) Sensor #2: multiple pseudo-error signals.

Fig. 7. Wave-form of the signal at each sensor and theoretical transient duration (blue dashed lines indicate the amplitude of the signal before control).

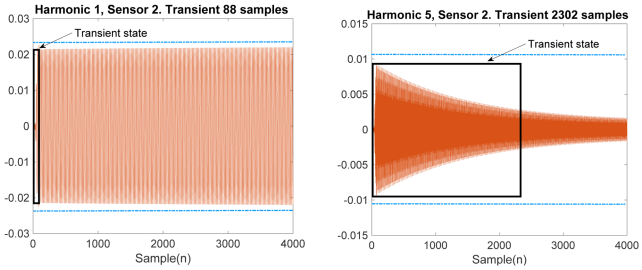

(a) Fastest convergence at sensor #2: multiple pseudo-error signal.

(b) Slowest convergence at sensor #2: multiple pseudo-error signal.

Fig. 8. Wave-forms of selected isolated harmonics at sensor #2 and theoretical transient duration (blue dashed lines indicate the amplitude of the signal before control, $\beta_{21} = 0.9$ and $\beta_{25} = 0.1$).

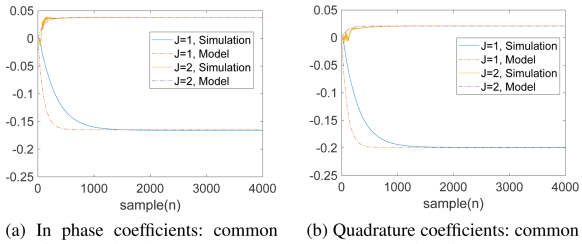

(a) In phase coefficients: common pseudo-error signal.

(b) Quadrature coefficients: common pseudo-error signal.

(c) In phase coefficients: multiple pseudo-error signal.

(d) Quadrature coefficients: multiple pseudo-error signal.

Fig. 9. Time evolution of a pair of filter coefficients corresponding to the third noise harmonic in comparison with the model given by (48).

model can suitably follow the coefficient transient evolution. These behaviour can be observed in all coefficient pairs.

V. Conclusion

A multi-channel active equalizer for multi-frequency noise signals, which allows different equalization gains for each sensor and for each frequency component of the noise, has been proposed. To this end, new pseudo-error signals have been defined that depend on the desired equalization profiles at each sensor, and on the weighting parameters of the output signals generated by the loudspeakers. We have obtained the expression of the optimal filter coefficients associated to every loudspeaker of the system in the case of single-frequency noise. However, taking into account that this solution requires the knowledge of the primary acoustic paths, we have alternatively proposed an adaptive strategy based on the LMS algorithm. Furthermore, we have extended the analysis performed for single-frequency noises to the case of multi-frequency noises. In this sense, two adaptive strategies have been derived: the first uses a common pseudo-error signal at each sensor, whereas the second proposes a different pseudo-error signal for each frequency at each sensor, which we have called multiple pseudo-error signal. Simulations have been carried out with real acoustic paths and they have shown that both strategies provide a similar behavior and manage to reach the desired equalization profiles at each sensor. However, it should be noted that the strategy based on the multiple pseudo-error signal may show uncontrolled influences in nearby frequencies, since it actually reaches its solution by solving an individual parallel problem for each frequency component. On the other hand the strategy based on a common pseudo-error signal achieves a global solution for all frequency components. Furthermore, it has been shown that the steady state behaviour of these algorithms and the duration of their transient stages can be estimated from the transfer function analysis. Together with the simulations, it has been also shown that the active controllers provided by the iterative strategies tend in practice to their corresponding theoretical values.

Appendix A
Multi-Channel ANE Adaptive Filtering Strategy Based on Common Pseudo-Error Signal

The optimal coefficients that minimize the mean square of the pseudo-error signal can be obtained as in Section II-A, but considering the new pseudo-error signal defined in (36). The signal recorded at each sensor is given by

$$e_k(n) = d_k(n) + \sum_{l=1}^{L}\sum_{j=1}^{J}(1-\gamma_{lj})\mathbf{x}_{ljk}^T(n)\mathbf{w}_{lj}(n). \quad (49)$$

Assuming perfect estimation of the secondary paths $\widetilde{\mathbf{x}}_{ljk}^T(n) = \mathbf{x}_{ljk}^T(n)$, then (36) can be expressed as

$$\begin{aligned} e'_k(n) &= d_k(n) + \sum_{l=1}^{L}\sum_{j=1}^{J}\frac{1-\gamma_{lj}}{1-\beta_{lk}}\mathbf{x}_{ljk}^T(n)\mathbf{w}_{lj}(n) \\ &= d_k(n) + \mathbf{x}_k^T(n)\mathbf{w}(n), \end{aligned} \quad (50)$$

where the $2LJ \times 1$ vector

$$\mathbf{x}_k(n) = \left[\frac{1-\gamma_{11}}{1-\beta_{1\,k}} \mathbf{x}_{11\,k}^T(n) \dots \frac{1-\gamma_{1J}}{1-\beta_{1\,k}} \mathbf{x}_{1Jk}^T(n) \dots \times \frac{1-\gamma_{L1}}{1-\beta_{Lk}} \mathbf{x}_{L1k}^T(n) \dots \frac{1-\gamma_{LJ}}{1-\beta_{Lk}} \mathbf{x}_{LJk}^T(n) \right]^T, \tag{51}$$

shares the notation with (21) but now it is formed by the extension of (21) to the case of L frequencies, and

$$\mathbf{w}(n) = \left[\mathbf{w}_{11}^T(n) \quad \dots \quad \mathbf{w}_{1J}^T(n) \quad \dots \quad \mathbf{w}_{L1}^T(n) \quad \dots \quad \mathbf{w}_{LJ}^T(n) \right]^T, \tag{52}$$

is a $2LJ \times 1$ vector with the same notation as in (18) but now formed by stacking the filter coefficients for the L frequencies ordered according to the expression of $\mathbf{x}_k(n)$ in (51).

Therefore, the optimal coefficients that minimize $\mathrm{E}\{(\mathbf{e}'(n))^T \mathbf{e}'(n)\}$ can be obtained as

$$\mathbf{w}_{opt} = -\mathbf{R}_{\mathrm{A}}^{-1} \mathbf{p}_{\mathrm{A}}, \tag{53}$$

where the $2LJ \times 2LJ$ augmented correlation matrix $\mathbf{R}_{\mathrm{A}}$ is defined as in (19) and (20) respectively, with dimensions $2LJ \times 2LJ$ for $\mathbf{R}_{\mathrm{A}}$ and $2LJ \times 1$ for $\mathbf{p}_{\mathrm{A}}$.

Taking into account that components belonging to different frequencies are uncorrelated, i.e. $\mathrm{E}\{\mathbf{x}_{ljk}\mathbf{x}_{mjk}\} = 0$ if $l \neq m$, then the augmented correlation matrix $\mathbf{R}_A$ is a block diagonal matrix:

$$\mathbf{R}_A = \begin{bmatrix} \mathbf{R}(\omega_1) & \mathbf{0}_{2J\times 2J} & \dots & \mathbf{0}_{2J\times 2J} \\ \mathbf{0}_{2J\times 2J} & \mathbf{R}(\omega_2) & \dots & \mathbf{0}_{2J\times 2J} \\ \vdots & & \ddots & \vdots \\ \mathbf{0}_{2J\times 2J} & \mathbf{0}_{2J\times 2J} & \dots & \mathbf{R}(\omega_L) \end{bmatrix}, \tag{54}$$

where every submatrix $\mathbf{R}(\omega_l)$ is defined in the same way as (22) but for ω_l, $l = 1, \dots, L$ and $\mathbf{0}_{2J\times 2J}$ is a square matrix with zero elements. For the sake of clarity we state here the expression of the 2×2 matrix $\mathbf{R}_{fc}(\omega_l)$ located at the f-th row and c-th column of the partition of $\mathbf{R}(\omega_l)$ as in (22):

$$\mathbf{R}_{fc}(\omega_l) = \sum_{k=1}^{K} \mathrm{E}\left\{ \frac{(1-\gamma_{lf})(1-\gamma_{lc})}{(1-\beta_{lk})^2} \mathbf{x}_{lfk}(n) \mathbf{x}_{lck}^T(n) \right\} = \sum_{k=1}^{K} G_{fclk} \begin{bmatrix} \cos(\phi_{lfk} - \phi_{lck}) & -\sin(\phi_{lfk} - \phi_{lck}) \\ \sin(\phi_{lfk} - \phi_{lck}) & \cos(\phi_{lfk} - \phi_{lck}) \end{bmatrix}, \tag{55}$$

where

$$G_{fclk} = \frac{(1-\gamma_{lf})(1-\gamma_{lc}) A_{\mathrm{ref},l}^2 A_{lfk} A_{lck}}{(1-\beta_{lk})^2}. \tag{56}$$

At this point the augmented cross-correlation vector $\mathbf{p}_{\mathrm{A}}$ follows the same composition of above, but for L frequencies. Thus it can be expressed as a partition of LJ subvectors of 2×1 elements:

$$\mathbf{p}_{\mathrm{A}} = \left[\mathbf{p}_1^T(\omega_1) \quad \dots \quad \mathbf{p}_J^T(\omega_1) \quad \dots \quad \mathbf{p}_1^T(\omega_L) \quad \dots \quad \mathbf{p}_J^T(\omega_L) \right]^T, \tag{57}$$

where

$$\mathbf{p}_j(\omega_l) = \sum_{k=1}^{K} \mathrm{E}\{\mathbf{x}_{ljk}(n) d_k(n)\} = \sum_{k=1}^{K} \frac{A_{\mathrm{ref},l}^2 A_{ljk} A_{lk} (1-\gamma_{lj})}{2(1-\beta_{lk})} \begin{bmatrix} \cos(\phi_{ljk} - \phi_{lk}) \\ \sin(\phi_{ljk} - \phi_{lk}) \end{bmatrix}.$$

It can be shown that the solution given by (53) for a particular ω_l is the same as the one obtained in Section II-A particularizing $w_0 = w_l$ in (27).

Considering now an adaptive strategy similar to that proposed for single-frequency signals in (28), we can express

$$\mathbf{w}(n) = \mathbf{w}(n-1) - \boldsymbol{\mu} \nabla_{\mathbf{w}} \{(\mathbf{e}'(n))^T \mathbf{e}'(n)\}, \tag{58}$$

where

$$\boldsymbol{\mu} = \mathrm{diag}\left\{ \underbrace{\mu_1, \dots, \mu_1}_{2J \text{ times}}, \underbrace{\mu_2, \dots, \mu_2}_{2J \text{ times}}, \dots, \underbrace{\mu_L, \dots, \mu_L}_{2J \text{ times}} \right\} \tag{59}$$

is a $2JL \times 2JL$ diagonal matrix formed by L different values $(\mu_1, \mu_2, \dots, \mu_L)$, with μ_l the step size for the frequency component ω_l. Dependence on l must be included in μ_l because different frequency components can exhibit different convergence conditions. Taking into account the generic expression of the pseudo-error signals given in (36), the updating (58) for the adaptive filter of loudspeaker j and l-th frequency can be expressed as

$$\mathbf{w}_{lj}(n) = \mathbf{w}_{lj}(n-1) - 2\mu_l \sum_{k=1}^{K} \frac{1-\gamma_{lj}}{1-\beta_{lk}} \mathbf{x}_{ljk}(n) e'_k(n). \tag{60}$$

Appendix B
Multi-Channel ANE Adaptive Filtering Strategy Based on Multiple Pseudo-Error Signals

Taking into account the expression of the error signal in (49), we can express the pseudo-error signal (41) as

$$e'_{lk}(n) = d_k(n) + \sum_{j=1}^{J} \left\{ \frac{1-\gamma_{lj}}{1-\beta_{lk}} \mathbf{x}_{ljk}^T(n) \mathbf{w}_{lj}(n) + \sum_{m \neq l} (1-\gamma_{mj}) \mathbf{x}_{mjk}^T(n) \mathbf{w}_{mj}(n) \right\}, \tag{61}$$

where we have split the different frequency components of (49) into two parts: one term containing the frequency component of interest, ω_l, which is affected by the equalization gain β_{lk}, and the other term including the rest of frequency components such that $m \neq l$. The pseudo-error signal in (61) can be expressed in compact form as

$$e'_{lk}(n) = d_k(n) + \mathbf{x}_k^T(n) \mathbf{w}(n), \tag{62}$$

where vector $\mathbf{w}(n)$ is given by (52) and $\mathbf{x}_k^T(n)$ is newly defined as

$$\begin{aligned}\mathbf{x}_k(n) = \big[&(1-\gamma_{11})\mathbf{x}_{l1\,k}^T(n)\ \ldots\ (1-\gamma_{1J})\mathbf{x}_{1Jk}^T(n)\ \ldots\\ &\times\frac{1-\gamma_{l1}}{1-\beta_{lk}}\mathbf{x}_{l1k}^T(n)\ \ldots\ \frac{1-\gamma_{lJ}}{1-\beta_{lk}}\mathbf{x}_{lJk}^T(n)\ \ldots\\ &\times(1-\gamma_{L1})\mathbf{x}_{L1k}^T(n)\ \ldots\ (1-\gamma_{LJ})\mathbf{x}_{LJk}^T(n)\big]^T.\end{aligned} \tag{63}$$

The above expression is similar to the expression of the common pseudo-error signal given by (50) except for the fact that (62) depends only on the equalization gain β_{lk} for the l-th frequency, as it can be seen from the definition of $\mathbf{x}_k(n)$ in (63). In this sense, the solution that gives the optimal coefficients that minimize $\mathrm{E}\{(\mathbf{e}'(n))^T\mathbf{e}'(n)\}$ is provided by (53), but the correlation matrix $\mathbf{R}_A$ and cross-correlation vector $\mathbf{p}_A$ have to be written according to the new definition of $\mathbf{x}_k(n)$ in (63). Therefore, the expression of the correlation matrix $\mathbf{R}_A$ is given by (54), but the $2J\times 2J$ submatrices $\mathbf{R}(\omega_m)$ are now partitioned into the following 2×2 submatrices:

$$\begin{aligned}&\mathbf{R}_{fc}(\omega_m)\\ &=\sum_{k=1}^{K}G_{fcmk}\begin{bmatrix}\cos(\phi_{mfk}-\phi_{mck}) & -\sin(\phi_{mfk}-\phi_{mck})\\ \sin(\phi_{mfk}-\phi_{mck}) & \cos(\phi_{mfk}-\phi_{mck})\end{bmatrix},\end{aligned} \tag{64}$$

where

$$G_{fcmk}=\frac{(1-\gamma_{mf})(1-\gamma_{mc})A_{\mathrm{ref},m}^2A_{mfk}A_{mck}}{(1-\beta'_{mk})^2} \tag{65}$$

and

$$\beta'_{mk}=\begin{cases}\beta_{mk} & m=l\\ 0 & m\neq l\end{cases}. \tag{66}$$

The expression of the cross-correlation vector $\mathbf{p}_A$ is given by (57), but the 2×1 subvectors of the partition are now expressed as

$$\begin{aligned}&\mathbf{p}_j(\omega_m)\\ &=\sum_{k=1}^{K}\frac{A_{\mathrm{ref},m}^2A_{mjk}A_{mk}(1-\gamma_{mj})}{2(1-\beta'_{mk})}\begin{bmatrix}\cos(\phi_{mjk}-\phi_{mk})\\ \sin(\phi_{mjk}-\phi_{mk})\end{bmatrix},\end{aligned} \tag{67}$$

where β'_{mk} is given by (66).

As said before, the advantage of this strategy based on multiple pseudo-error signals relies on the possibility of updating the filter coefficients independently for every frequency component. In order to state the adaptive algorithm that converge to the above solution, let us define the $2J\times 1$ partition of $\mathbf{w}(n)$ in (52) that contains the filter coefficients affecting only to the frequency component ω_l as

$$\mathbf{w}_l^{(2J)}(n)=\begin{bmatrix}\mathbf{w}_{l1}^T(n) & \ldots & \mathbf{w}_{lJ}^T(n)\end{bmatrix}^T. \tag{68}$$

The gradient algorithm is then expressed by

$$\mathbf{w}_l^{(2J)}(n)=\mathbf{w}_l^{(2J)}(n-1)-\mu_l\nabla_{\mathbf{w}_l^{(2J)}}\{(\mathbf{e}'_l(n))^T\mathbf{e}'_l(n)\}, \tag{69}$$

where $\mathbf{e}'_l=\begin{bmatrix}e'_{l1} & \ldots & e'_{lK}\end{bmatrix}^T$.

In a similar way to (37), the updating equation can be stated as

$$\mathbf{w}_{lj}(n)=\mathbf{w}_{lj}(n-1)-2\mu_l\sum_{k=1}^{K}\frac{1-\gamma_{lj}}{1-\beta_{lk}}\mathbf{x}_{ljk}(n)e'_{lk}(n), \tag{70}$$

for ω_l with $l=1,\ldots,L$. The above expression can be rewritten in compact form for the whole set of filter coefficients for the given frequency component ω_l as

$$\mathbf{w}_l^{(2J)}(n)=\mathbf{w}_l^{(2J)}(n-1)-2\mu_l\sum_{k=1}^{K}\mathbf{x}_{lk}^{(2J)}(n)e'_{lk}(n), \tag{71}$$

where $\mathbf{x}_{lk}^{(2J)}(n)$ is the $2J\times 1$ partition of vector $\mathbf{x}_k(n)$ in (63) such that

$$\mathbf{x}_{lk}^{(2J)}(n)=\begin{bmatrix}\frac{1-\gamma_{l1}}{1-\beta_{lk}}\mathbf{x}_{l1k}^T(n) & \ldots & \frac{1-\gamma_{lJ}}{1-\beta_{lk}}\mathbf{x}_{lJk}^T(n)\end{bmatrix}^T. \tag{72}$$

Appendix C
Convergence in Mean of the Adaptive Multiple Pseudo-Error Equalizer Algorithm

Assuming perfect acoustic path estimation, the filter updating equation, (71), can be rewritten in matrix form as

$$\begin{aligned}\mathbf{w}_l^{(2J)}(n)=\ &\mathbf{w}_l^{(2J)}(n-1)\\ &-2\mu_l[\mathbf{x}_{l1}^{(2J)}(n)\ \ldots\ \mathbf{x}_{lK}^{(2J)}(n)]\mathbf{e}'_l(n),\end{aligned}$$

where vector $\mathbf{e}'_l(n)$ can be written, following (61), as

$$\mathbf{e}'_l(n)=\mathbf{d}(n)+\sum_{m=1}^{L}\begin{bmatrix}(\mathbf{x}_{m1}^{(2J)}(n))^T\\ \vdots\\ (\mathbf{x}_{mK}^{(2J)}(n))^T\end{bmatrix}\mathbf{w}_m^{(2J)}(n), \tag{73}$$

and vector $\mathbf{d}(n)$ is defined as $\mathbf{d}(n)=[d_1(n)\ \ldots\ d_k(n)]^T$. Vectors $\mathbf{x}_{mk}^{(2J)}(n)$ are defined as in (72) for $m=l$, but when $m\neq l$, $\mathbf{x}_{mk}^{(2J)}(n)$ are defined as in (72) with $\beta_{mk}=0$.

Applying the expectation operator in (73) and considering that

$$\mathbf{w}_l^{(2J)}(n)=\mathbf{w}_l^{(2J)}(n-1)=\mathbf{w}_l^{(2J)}[\infty] \tag{74}$$

when $n\to\infty$, then

$$\begin{aligned}&\mathrm{E}\left\{[\mathbf{x}_{l1}^{(2J)}(n)\ \ldots\ \mathbf{x}_{lK}^{(2J)}(n)]\mathbf{d}(n)\right\}\\ &+\mathrm{E}\left\{[\mathbf{x}_{l1}^{(2J)}(n)\ \ldots\ \mathbf{x}_{lK}^{(2J)}(n)]\sum_{m=1}^{L}\begin{bmatrix}(\mathbf{x}_{m1}^{(2J)}(n))^T\\ \vdots\\ (\mathbf{x}_{mK}^{(2J)}(n))^T\end{bmatrix}\right.\\ &\left.\times\,\mathbf{w}_m^{(2J)}[\infty]\right\}=0.\end{aligned} \tag{75}$$

Since tonal signals are uncorrelated for different frequencies, that is, $\mathrm{E}\{\mathbf{x}_{lq}^{(2J)}(n)(\mathbf{x}_{mk}^{(2J)}(n))^T\} = 0, \forall q, \forall k$ when $m \neq l$, it is fulfilled that

$$\mathrm{E}\left\{[\mathbf{x}_{l1}^{(2J)}(n) \ \dots \ \mathbf{x}_{lK}^{(2J)}(n)]\mathbf{d}(n)\right\} + \mathrm{E}\left\{[\mathbf{x}_{l1}^{(2J)}(n) \ \dots \ \mathbf{x}_{lK}^{(2J)}(n)]\begin{bmatrix}(\mathbf{x}_{l1}^{(2J)}(n))^T \\ \vdots \\ (\mathbf{x}_{lK}^{(2J)}(n))^T\end{bmatrix}\right\} \times \mathbf{w}_l^{(2J)}[\infty] = 0. \tag{76}$$

Using the definitions introduced in Section III-B, the above expression can be rewritten as

$$\left[\mathbf{p}_1^T(\omega_l) \ \dots \ \mathbf{p}_J^T(\omega_l)\right]^T + \mathbf{R}(\omega_l)\mathbf{w}_l^{(2J)}[\infty] = 0, \tag{77}$$

and

$$\mathbf{w}_l^{(2J)}[\infty] = -\mathbf{R}(\omega_l)^{-1}\left[\mathbf{p}_1^T(\omega_) \ \dots \ \mathbf{p}_J^T(\omega_l)\right]^T. \tag{78}$$

On the other hand, (53) can be solved for all the frequency components, $l \in \{1, \dots, L\}$, based on the definitions proposed in Section III-B to minimize $\mathrm{E}\{\mathbf{e}_l'^T(n)\mathbf{e}_l'(n)\}$, thus

$$\begin{bmatrix}\mathbf{w}_{1,opt} \\ \mathbf{w}_{2,opt} \\ \vdots \\ \mathbf{w}_{L,opt}\end{bmatrix} = -\begin{bmatrix}\mathbf{R}(\omega_1) & \mathbf{0}_{2J\times 2J} & \dots & \mathbf{0}_{2J\times 2J} \\ \mathbf{0}_{2J\times 2J} & \mathbf{R}(\omega_2) & \dots & \mathbf{0}_{2J\times 2J} \\ \vdots & & \ddots & \vdots \\ \mathbf{0}_{2J\times 2J} & \mathbf{0}_{2J\times 2J} & \dots & \mathbf{R}(\omega_L)\end{bmatrix}^{-1} \times \begin{bmatrix}\mathbf{p}(\omega_1) \\ \mathbf{p}(\omega_2) \\ \vdots \\ \mathbf{p}(\omega_L)\end{bmatrix}, \tag{79}$$

where $\mathbf{p}(\omega_l) = [\mathbf{p}_1^T(\omega_l) \ \dots \ \mathbf{p}_J^T(\omega_l)]^T$.

Finally, the following identity can be stated comparing (78) and (79):

$$\mathbf{w}_l^{(2J)}[\infty] = \mathbf{w}_{l,opt} = -\mathbf{R}(\omega_l)^{-1}\mathbf{p}(\omega_l). \tag{80}$$

It should be noted that the mean values of submatrices $\mathbf{R}_{fc}(\omega_l)$ of matrix $\mathbf{R}(\omega_l)$ coincide for the case of the common pseudo-error in (55) and the multiple pseudo-error in (64).

REFERENCES

[1] Y. Huang, T. Chen, and P. Shieh, "Analytical estimation of the noise due to a rotating shaft," *Appl. Acoust.*, vol. 76, pp. 187–196, 2014. [Online]. Available: https://www.sciencedirect.com/science/article/pii/S0003682X13001904

[2] J. Glover, "Adaptive noise canceling applied to sinusoidal interferences," *IEEE Trans. Acoust., Speech, Signal Process.*, vol. 25, no. 6, pp. 484–491, Dec. 1977.

[3] S. Kuo, X. Kong, S. Chen, and W. Hao, "Analysis and design of narrowband active noise control systems," in *Proc. IEEE Int. Conf. Acoust., Speech Signal Process.*, vol. 6, 1998, pp. 3557–3560.

[4] H. Jeon, T. Chang, and S. Kuo, "A narrowband active noise control system with frequency corrector," *IEEE Trans. Audio, Speech, Lang. Process.*, vol. 19, pp. 990–1002, May 2011.

[5] C.-Y. Chang and S. M. Kuo, "Complete parallel narrowband active noise control systems," *IEEE Trans. Audio, Speech, Lang. Process.*, vol. 21, no. 9, pp. 1979–1986, Sep. 2013.

[6] T. Wang, W. Gan, and S. Kuo, "New feedback active noise control system with improved performance," in *Proc. IEEE Int. Conf. Acoust., Speech, Signal Process.*, 2014, pp. 6662–6666.

[7] P. A. C. Lopes and J. A. B. Gerald, "A narrowband active noise control system with reference synthesis," *Int. J. Adaptive Control Signal Process.*, vol. 33, no. 7, pp. 1118–1133, 2019. [Online]. Available: https://onlinelibrary.wiley.com/doi/abs/10.1002/acs.3011

[8] H. Wang, H. Sun, Y. Sun, M. Wu, and J. Yang, "A narrowband active noise control system with a frequency estimation algorithm based on parallel adaptive notch filter," *Signal Process.*, vol. 154, pp. 108–119, 2019. [Online]. Available: https://www.sciencedirect.com/science/article/pii/S0165168418302731

[9] M. T. Akhtar, "Narrowband feedback active noise control systems with secondary path modeling using gain-controlled additive random noise," *Digit. Signal Process.*, vol. 111, 2021, Art. no. 102976. [Online]. Available: https://www.sciencedirect.com/science/article/pii/S1051200421000154

[10] A. Gonzalez, M. Ferrer, M. de Diego, and G. Piñero, "Subjective considerations in multichannel active noise control equalization of repetitive noise," *Proc. ACTIVE*, vol. 1, pp. 387–397, Jul. 2002.

[11] P. Benois and U. Zolzer, "Psychoacoustic optimization of a feedback controller for active noise cancelling headphones," in *Proc. 26th Int. Congr. Sound Vib.*, Montreal, Canada, 2019, pp. 356–363.

[12] V. Belyi and W.-S. Gan, "Integrated psychoacoustic active noise control and masking," *Appl. Acoust.*, vol. 145, pp. 339–348, 2019.

[13] N. Bershad and J. Bermudez, "Sinusoidal interference rejection analysis of an LMS adaptive feedforward controller with a noisy periodic reference," *IEEE Trans. Signal Process.*, vol. 46, no. 5, pp. 1298–1313, May 1998.

[14] J. Estreder, G. Piñero, M. Ferrer, M. de Diego, and A. Gonzalez, "Perceptual active equalization of multi-frequency noise," in *Proc. 18th Int. Conf. Signal Process. Multimedia Appl.*, 2021, pp. 39–47.

[15] M. J. Ji and S. M. Kuo, "An active harmonic noise equalizer," in *Proc. Int. Conf. Acoust., Speech Signal Process.*, vol. 1, 1993, pp. 189–192..

[16] S. M. Kuo, M. J. Ji, and X. H. Jiang, "Development and experiment of narrowband active noise equalizer," *Noise Control Eng. J.*, vol. 41, no. 3, pp. 281–288, Jul./Aug. 1993.

[17] L. Rees and S. Elliott, "Adaptive algorithms for active sound-profiling," *IEEE Trans. Audio, Speech, Lang. Process.*, vol. 14, no. 2, pp. 711–719, Mar. 2006.

[18] V. Patel, J. Cheer, and N. V. George, "Modified phase-scheduled-command FxLMS algorithm for active sound profiling," *IEEE/ACM Trans. Audio, Speech, Lang. Process.*, vol. 25, no. 9, pp. 1799–1808, Sep. 2017.

[19] S. Ryu, J. Kim, and Y.-S. Lee, "Active sound profiling of narrowband signals for improving sound quality in an enclosed space," *Multimedia Tools Appl.*, vol. 76, pp. 24595–24607,2017.

[20] S. M. Kuo, M. Tahernezhadi, and W. Hao, "Convergence analysis of narrow-band active noise control system," *IEEE Trans. Circuits Syst. II, Analog Digit. Signal Process.*, vol. 46, pp. 220–223, Feb. 1999.

[21] S. Kim and Y. Park, "On-line fundamental frequency tracking method for harmonic signal and application to anc," *J. Sound Vib.*, vol. 241, pp. 681–691, 2001.

[22] C.-Y. Ho, K.-K. Shyu, C.-Y. Chang, and S. M. Kuo, "Efficient narrowband noise cancellation system using adaptive line enhancer," *IEEE/ACM Trans. Audio, Speech, Lang. Process.*, vol. 28, pp. 1094–1103, 2020.

[23] T. Wang, W.-S. Gan, and S. M. Kuo, "New feedback active noise control system with improved performance," in *Proc. IEEE Int. Conf. Acoust., Speech, Signal Process.*, 2014, pp. 6662–6666.

[24] H. Jeon, T. Chang, and S. Kuo, "Analysis of frequency mismatch in narrowband active noise control," *IEEE Trans. Acoust., Speech, Signal Process.*, vol. 18, pp. 1632–1642, Aug. 2010.

[25] S. Kuo and S. Nallabolu, "Analysis and correction of frequency error in electronic mufflers using narrowband active noise control," in *Proc. IEEE Int. Conf. Control Appl.*, 2007, pp. 1353–1358.

[26] J. Liu and X. Chen, "Adaptive compensation of misequalization in narrowband active noise equalizer systems," *IEEE/ACM Trans. Audio, Speech, Lang. Process.*, vol. 24, no. 12, pp. 2390–2399, Dec. 2016.

[27] L. Luo, J. Sun, B. Huang, and D. Quoc, "Efficient combination of feedforward and feedback structures for nonlinear narrowband active noise control," *Signal Process.*, vol. 128, pp. 494–503, Nov. 2016.

[28] S. Kuo, "Multiple-channel adaptive noise equalizers," in *Proc. Conf. Rec. 29th Asilomar Conf. Signals, Syst. Comput.*, vol. 2, 1995, pp. 1250–1254.

[29] M. de Diego, A. Gonzalez, M. Ferrer, and G. Piñero, "Performance comparison of multichannel active noise control equalizers," *Proc. ACTIVE*, vol. 1, pp. 413–424, Jul. 2002.

[30] M. de Diego, A. Gonzalez, M. Ferrer, and G. Piñero, "Multichannel active noise control system for local spectral reshaping of multifrequency noise," *J. Sound Vib.*, vol. 274, no. 1, pp. 249–271, 2004.

[31] S. Elliott, I. Stothers, and P. Nelson, "A multiple error LMS algorithm and its application to the active control of sound and vibration," *IEEE Trans. Acoust., Speech, Signal Process.*, vol. 35, no. 10, pp. 1423–1434, Oct. 1987.
[32] A. Gonzalez, M. de Diego, M. Ferrer, and G. Piñero, "Multichannel active noise equalization of interior noise," *IEEE Trans. Audio, Speech, Lang. Process.*, vol. 14, no. 1, pp. 110–122, Jan. 2006.
[33] S. M. Kuo and M. J. Ji, "Development and analysis of an adaptive noise equalizer," *IEEE Trans. Speech Audio Process.*, vol. 3, no. 3, pp. 217–222, May 1995.
[34] E. Bjarnason, "Analysis of the filtered-X LMS algorithm," *IEEE Trans. Speech Audio Process.*, vol. 3, no. 6, pp. 504–514, Nov. 1995.
[35] N. Mohseni, T. W. Nguyen, S. A. Ul Islam, I. V. Kolmanovsky, and D. S. Bernstein, "Active noise control for harmonic and broadband disturbances using RLS-based model predictive control," in *Proc. Amer. Control Conf.*, 2020, pp. 1393–1398.
[36] M. Bekrani and M. Lotfizad, "Clipped LMS/RLS adaptive algorithms: Analytical evaluation and performance comparison with low-complexity counterparts," *Circuits, Syst. Signal Process.*, vol. 34, pp. 1655–1682, 2015.
[37] M. Bekrani, R. Bibak, and M. Lotfizad, "Improved clipped affine projection algorithm," *IET Signal Process.*, vol. 13, no. 1, pp. 103–111, 2019.
[38] B. Widrow and S. D. Stearns, *Adaptive Signal Processing*. Englewood Cliffs, NJ, USA: Prentice-Hall, 1985.
[39] J. Vanderkooy, "Aspects of MLS measuring systems," *J. Audio Eng. Soc.*, vol. 42, no. 4, pp. 219–231, 1994.
[40] A. Farina, "Simultaneous measurement of impulse response and distortion with a swept-sine technique," in *Proc. Audio Eng. Soc. Conv.*, 2000, Paper 5093. [Online]. Available: http://www.aes.org/e-lib/browse.cfm?elib=10211
[41] C.-Y. Chang, S. M. Kuo, and C.-W. Huang, "Secondary path modeling for narrowband active noise control systems," *Appl. Acoust.*, vol. 131, pp. 154–164, 2018. [Online]. Available: https://www.sciencedirect.com/science/article/pii/S0003682X17307302
[42] M. Ferrer, M. de Diego, G. Piñero, A. Hassani, M. Moonen, and A. Gonzalez, "Transfer functions of fxlms-based multi-channel multi-tone active noise equalizers," 2022. [Online]. Available: https://arxiv.org/abs/2207.01102
[43] "Loudspeaker and microphone setup at the GTAC listening room," [Online]. Available: http://www.gtac.upv.es/room.php

Miguel Ferrer Contreras (Member, IEEE) received the Graduation degree in telecommunications engineering from Universidad Politécnica de Valencia (UPV), Valencia, Spain, in 2000. Since a year before, he has been collaborating with the Audio and Communications Signal Processing Group (GTAC) performing a six months research stay with Instituto de Investigación Aplicada al Automóvil, Tarragona, Spain (Automobile Applied Research Institute). Subsequently, he was the recipient of several grants offered both by the Communications Department of the UPV and by the Research, Development and Innovation Vice-Chancellery of the same university, enabling him to start his Doctorate studies and to collaborate in different Research Projects within the GTAC. During this period he has authored or co-authored more than seventy papers related with signal processing in renowned journals and conferences.

Since 2005, he has been an Assistant Lecturer with the Communications Department, Polytechnic University of Valencia (UPV) teaching different subjects related with Signal Processing and Communications. His research interests include the study of adaptive algorithms and its application to audio digital processing and noise active control, a subject about which he developed his doctoral thesis, and he continues to develop his research work with the GTAC, now belonging to the Institute of Telecommunications and Multimedia Applications (iTEAM) of the UPV.

Maria de Diego (Senior Member, IEEE) received the M.Sc. degree in telecommunications engineering and the Ph.D degree from the Universitat Politècnica de València, Valencia, Spain, in 1994 and 2003, respectively. She is currently an Associate Professor of digital signal processing and communications and a Researcher with the GTAC Group, Institute of Telecommunications and Multimedia Applications, Universitat Politècnica de València. She has been involved in more than 30 Research Projects financed by public funds, and she has led several of them. Her Ph.D research was mainly on adaptive equalization algorithms with applications to multifrequency noise control in enclosed spaces. Her Postdoctoral Research involved the development of signal processing algorithms for sound applications. She has also published some works on the topic of signal processing for communications. She is the author of more than 30 journal papers listed in the Journal Citation Reports, and around 50 conference papers. She is the Member of the International Institute of Acoustics and Vibration, having been elected to the board of directors during the periods 2015–2019 and 2022–2026. Dr. de Diego was an Associate editor for the IEEE/ACM TRANSACTIONS ON AUDIO, SPEECH, AND LANGUAGE (2018–2021). Her research interests include active noise control and equalization systems, distributed sound processing, non-linear adaptive filtering, audio applications over wireless acoustic networks, and finally sound quality and psychoacoustics.

Amin Hassani (Senior Member, IEEE) received the Ph.D. degree from the Department of Electrical Engineering (ESAT) division STADIUS center for dynamical systems, signal processing and data analytics (STADIUS), KU Leuven, Belgium, in 2017. Between 2017 and 2019, he was appointed as a Postdoctoral Research Associate with KU Leuven-ESAT-STADIUS, during which he was a Scientific Project Manager with the H2020-FET Project D-NOISE. Between 2019 and 2021, he was involved in an Exploitation Project within STADIUS to design cooperative signal processing solutions for IoT-based multi-user speech communication systems. In 2021, he Co-Founded CONNEXOUNDS as a spin-off company of KU Leuven, where he is currently the CEO and Technology Architect. He is also engaged with ESAT-STADIUS as a Guest Researcher. His research interests include distributed algorithm design and validation for real-time audio signal processing and speech enhancement.

Marc Moonen (Fellow, IEEE) is currently the Full Professor with the Electrical Engineering Department, KU Leuven, where he is also heading a Research Team working with the area of numerical algorithms and signal processing for digital communications, wireless communications, DSL and audio signal processing. He was the Chairman of the IEEE Benelux Signal Processing Chapter (1998–2002), Member of the IEEE Signal Processing Society Technical Committee on Signal Processing for Communications, and the President of EURASIP (European Association for Signal Processing, 2007–2008 and 2011–2012). He is also the Vice-President for Publications of the IEEE Signal Processing Society (2021–2023). He was the Editor-in-Chief of the *EURASIP Journal on Applied Signal Processing* (2003–2005), Area Editor of Feature Articles in IEEE Signal Processing Magazine (2012–2014), and has been Member of the Editorial Board of IEEE TRANSACTION CIRCUITS & SYSTEMS II (2002–2003), IEEE Signal Processing Magazine (2003–2005), Integration (1992–2005), Signal Processing (2007–2011), *EURASIP Journal Wireless Comms and Networking* (2003-2011), *EURASIP Journal Advances in Signal Processing* (2006–2016). He is a Fellow of EURASIP (2018). He was the recipient of the 1994 KU Leuven Research Council Award, and was a 1997 Laureate of the Belgium Royal Academy of Science. He was also the recipient of the 1997 Alcatel Bell (Belgium) Award (with Piet Vandaele), 2004 Alcatel Bell (Belgium) Award (with Raphael Cendrillon), 2008 CELTIC Excellence Award for EU/CELTIC Project 'BANITS', and 2020 EURASIP Meritorious Service Award, and also Two Journal Best Paper awards from the IEEE TRANSACTIONS ON SIGNAL PROCESSING (with Geert Leus and with Daniele Giacobello), One Journal Best Paper Award from *Elsevier Signal Processing* (with Simon Doclo), and Seven Conference Best Paper awards.

Gema Piñero (Senior Member, IEEE) received the M.Sc. degree in electrical engineering from the Technical University of Madrid, Madrid, Spain, in 1990, and the Ph.D. degree in electrical engineering from the Technical University of Valencia (UPV), Valencia, Spain, in 1997. She is currently a Full Professor with the UPV. Since 1995, she has led or contributed to 40 private and public funded projects on array signal processing for acoustics and communications, active noise control, personal sound zones and psychoacoustics. From 2013 to 2016, she was with the Spanish Chapter of the IEEE Women in Engineering. From 2015 to 2021, she was the part of the Editorial Board of the Digital Signal Processing Journal. She is also Visiting Professor with the University of Illinois at Urbana-Champaign, Champaign, IL, USA, in 2011, and with the Imperial College London in 2016. She has co-authored more than 90 papers in international journals and conferences, serving in the Technical Committee of some of them. Her research interest include machine learning for acoustics. She is the Member of the EURASIP and Founding Member of the Spanish Association for Research and Teaching Universitas.

Alberto Gonzalez (Senior Member, IEEE) received the Graduate degree (with Hons.) in telecommunication engineering from the Universitat Politecnica Catalunya, Barcelona, Spain, in 1991, and the Ph.D. degree *(magna cum laude)* from the Universitat Politècnica València, Valencia, Spain, in 1997. During 1995, he was a Visiting Researcher with the Institute of Sound and Vibration Research, University of Southampton, Southampton, U.K. He is currently heading a Research Group with audio and communications digital signal processing. He has authored and coauthored works in international technical journals and renowned conferences in the fields of signal processing and applied acoustics. Since June 2012 to December 2020, he has been Dean of the Telecommunication Engineering School, Universitat Politecnica Valencia. His research interests include optimization of computation methods for detection and decoding in digital communications and for distributed sound signal processing. He belonged to the EURASIP Special Area Team on Acoustic, Speech and Music Signal Processing.